Supporting Information

Kelley et al. 10.1073/pnas.1421533112

The Drought, Regional Climate Variability, and Trends

Fig. S1 is a timeline summarizing the events that preceded the Syrian uprising and also shows the addition of Iraqi refugees and Syrian IDPs to Syria's urban population from 2003 to 2010.

Applying a linear fit to the Global Precipitation Climatology Centre timeseries as with the CRU data yields a much larger (37%) reduction in rainfall since 1901 than for the CRU. This difference is primarily due to a lack of agreement during the first 30 years, when station data were quite sparse for Syria and this region (gray shading, Fig. 1*A*). The agreement after 1950 is quite good; the two data sets agree that the reduction from 1951 to 2008 was between 17% and 20%. Even the more conservative CRU estimate of a 13% (~6 mm/month) reduction since 1901 is nearly as large as the SD of the timeseries (~9 mm/month). Due to the increased uncertainty during the first 30 years, the linear least-squares fit from 1931 to 2008 is shown in Fig. 1*A*, and was also found to be significant ($P < 0.05$).

The globally gridded CRU data rely strongly on interpolation techniques where station data are sparse; Empirical Orthogonal Function (EOF) analysis of winter-to-winter precipitation was performed to compare with the GHCN stations from 1951 to 1990, the period during which the station density for this domain was largest, and the patterns were found to be consistent.

Fig. S2 shows the 6-month winter and summer timeseries of Syrian area mean surface temperature (CRU), for comparison with the annual surface temperature shown in Fig. 1*B*. As mentioned in *Regional Climate Variability and Trend*, the change over the 109 years is slightly larger during the summer half year (1.2 degrees) than during winter (0.9 degrees), and the summer trend is of particularly importance as this is the season of highest evaporation.

Frequency of Multiyear Droughts

Regression onto the observed curve of annual global atmospheric carbon dioxide (CO_2) mixing ratios is only one possible way to represent the response to the nonlinear forcing, or signal. Kelley et al. instead used a signal-to-noise maximizing EOF technique to extract the precipitation response signal common to all CMIP3 (and CMIP5) historical models over the greater Mediterranean region (1, 2). This model-estimated signal closely resembled the smoothed CO_2 curve, implying that, for this region, the precipitation response to the anthropogenic forcing closely resembles the forcing itself and has already begun to emerge from the natural variability.

Fig. S3 is a scatterplot comparing 16 CMIP5 model climatologies and winter-to-winter SDs, for both the historical and histNat experiments, before normalization.

Mechanisms

The theoretical mechanisms for drying of subtropical regions and for this region in particular agree with observations and with model simulations and projections and imply a rise in regional sea-level pressure (SLP) as a consequence of anthropogenic climate change. These mechanisms include both a thermodynamic component related to increased moisture-carrying capacity in a warmer atmosphere globally (3, 4) and a dynamical component involving an expanding Hadley Cell and a poleward migration of the midlatitude storm tracks (5–7), and more local processes specifically involving the Mediterranean storm track (8–11). A poleward migration, weakening, or suppressed development of the winter storms that enter Syria from the Mediterranean Sea would mean a reduction in winter rainfall, with potentially dire consequences for agriculture. Much of Syrian precipitation depends on cyclogenesis in the region of the Cyprus low and is associated with cold air outbreaks from Europe (10). A detailed analysis of the large-scale atmospheric conditions present during the record dry 2007/2008 winter (December–March) using the National Centers for Environmental Prediction/National Center for Atmospheric Research reanalysis (12) concluded that anomalous high surface pressure inhibited synoptic activity over the FC, and was accompanied by dry advection from the east and northeast that significantly reduced precipitable water and convective instability (10).

Observationally based data from the Twentieth Century Reanalysis show an increase in FC SLP since 1901. Although the linear trend is only marginally significant ($P < 0.14$), 40 years had elapsed, before the winter of 2009/2010, since the last recorded winter with SLP more than 1 SD below the 1901–1970 mean, while in the prior 70 winters, SLP regularly fell below this threshold (Fig. S4).

Distributions of observed 3-year running means of winter SLP over the Eastern Mediterranean (EM) indicate a similar difference as with precipitation between the total and residual after the CO_2 fit is removed. Extreme 3-year high-pressure events increase in frequency and intensity under the CO_2 forcing, and the most extreme events only occur when the strong NAO-related natural variability and the CO_2 forcing combine.

Further analysis of the CMIP5 simulations also points to the importance of anthropogenic forcing in the drying of the EM. The CMIP5 20th century multimodel mean gives a reduction in winter rainfall over Syria between 1901 and 2005 of 3–9%, compared with the CRU decrease of 2–10% (Fig. 1*A*). The CMIP5 model-simulated drying of the EM is consistent with the recent observed FC precipitation and EM SLP change. The CMIP5 multimodal mean of area-averaged EM SLP agrees with the observations in trending upward during the century, and the model projects this trend to continue strongly through the 21st century (Fig. S4). More generally, the projection for the 21st century under increased greenhouse gas forcing is for an increase in surface pressure and anticyclonic tendency, a reduction in the frequency and strength of cyclones in the EM, and a reduction in winter precipitation in the FC. For the 21st century model projections, we used the Representative Concentration Pathway experiment "rcp85," with an increase in radiative forcing of 8.5W/m^2 by 2100.

1. Kelley C, Ting M, Seager R, Kushnir Y (2012) The relative contributions of radiative forcing and internal climate variability to the late 20th century winter drying of the Mediterranean region. *Clim Dyn* 38:2001–2015.
2. Kelley C, Ting M, Seager R, Kushnir Y (2012) Mediterranean precipitation climatology, seasonal cycle, and trend as simulated by CMIP5. *Geophys Res Lett* 39:L21703.
3. Held IM, Soden BJ (2006) Robust responses of the hydrological cycle to global warming. *J Clim* 19(21):5686–5699.
4. Seager R, Naik N, Vecchi GA (2010) Thermodynamic and dynamic mechanisms for large-scale changes in the hydrological cycle in response to global warming. *J Clim* 23(17):4651–4668.
5. Lu J, Vecchi GA, Reichler TA (2007) Expansion of the Hadley cell under global warming. *Geophys Res Lett* 34:L06805.
6. Wu Y, Ting MF, Seager R, Huang H, Cane M (2011) Changes in storm tracks and energy transports in a warmer climate simulated by the GFDL CM2.1 model. *Clim Dyn* 37(1-2):53–72.
7. Yin JH (2005) A consistent poleward shift of the storm tracks in simulations of 21st century climate. *Geophys Res Lett* 32:L18701.
8. Trigo RM, Gouveia CM, Barriopedro D (2010) The intense 2007–2009 drought in the Fertile Crescent: Impacts and associated atmospheric circulation. *Agric Meteorol* 150:1245–1257.

9. Bengtsson L, Hodges K, Roeckner E (2006) Storm tracks and climate change. *J Clim* 19:3518–3543.
10. Lionello P, Giorgi F (2007) Winter precipitation and cyclones in the Mediterranean region: Future climate scenarios in a regional simulation. *Adv Geosci* 12: 153–158.
11. Ziv B, Kushnir Y, Nakamura J, Naik NH, Harpaz T (2013) Coupled climate model simulations of Mediterranean winter cyclones and large-scale flow patterns. *Nat Hazard Earth Sys* 13:779–793.
12. Kalnay E, et al. (1996) The NCEP/NCAR 40-year reanalysis project. *Bull Am Meteorol Soc* 77:437–471.

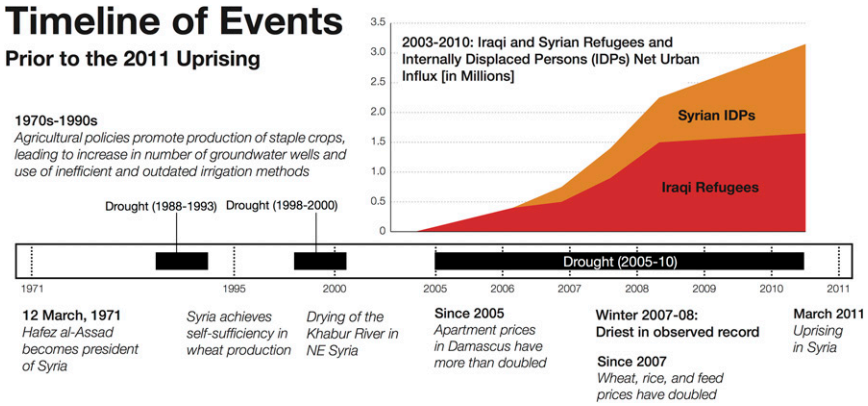

Fig. S1. Timeline of events leading up to the civil uprising that began in March 2011, along with a graph depicting the net urban influx (in millions) of Syrian IDPs and Iraqi refugees since 2005.

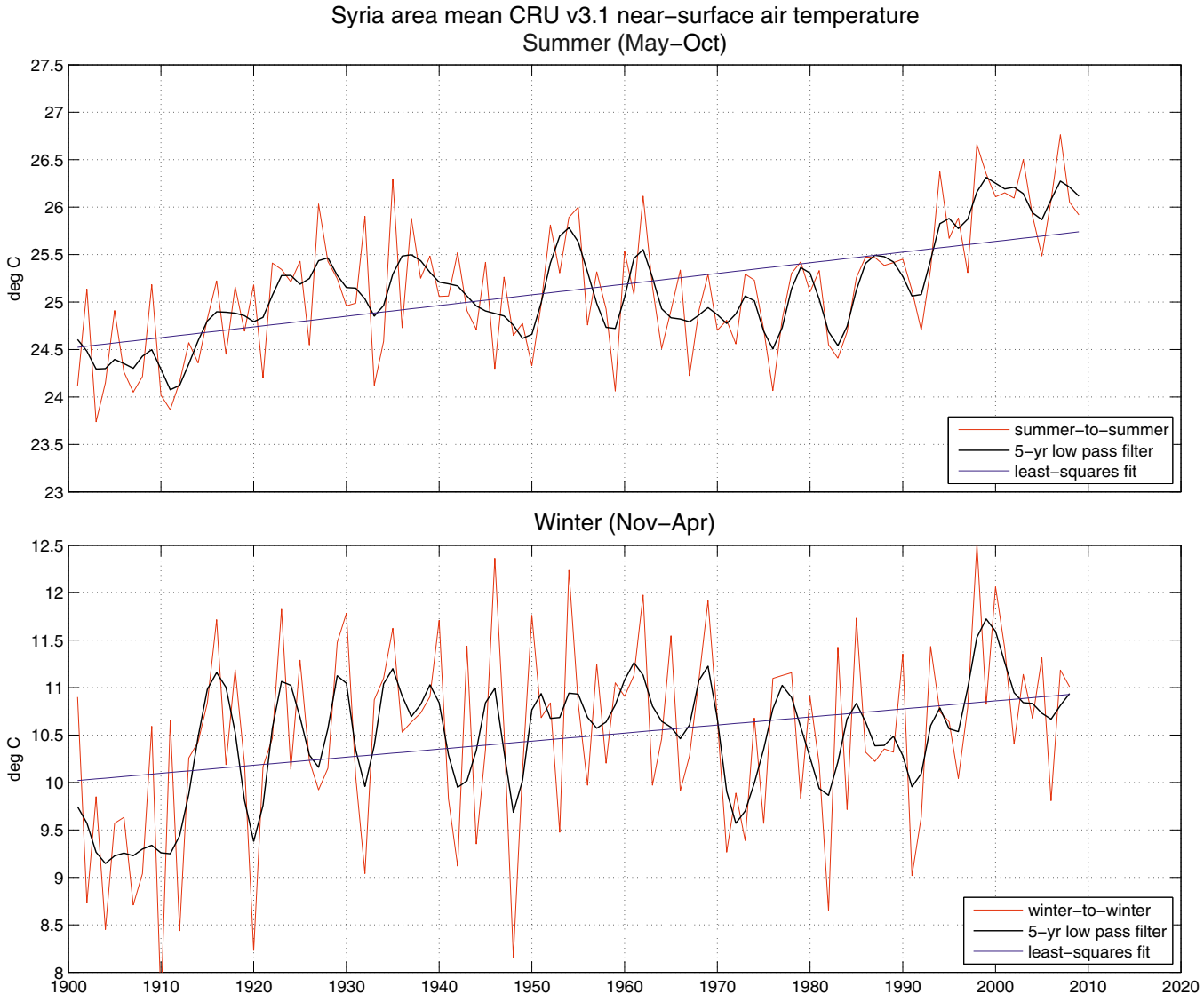

Fig. S2. Observed summer (May−October) and winter (November−April) near-surface temperature for the Syria area mean, CRU 3.1 data, with 5-year Butterworth low-pass filter (black) and least squares fit (blue).

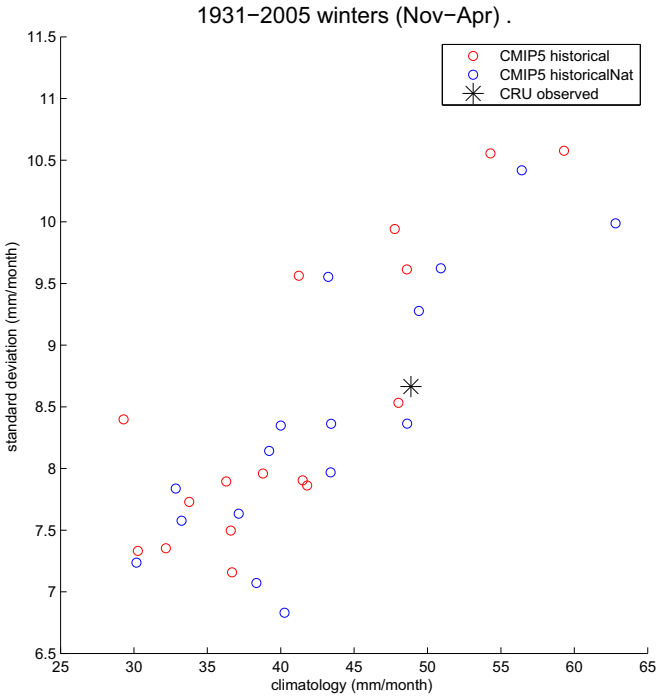

Fig. S3. Scatterplot intercomparison of 16 CMIP5 models (see Table S1) for the FC area mean 6-month winter (November–April) climatology and winter-to-winter SD from 1931 to 2005, with CRUv3.1 observed shown as an asterisk. Historical simulations are shown in red, and historicalNat simulations are shown in blue.

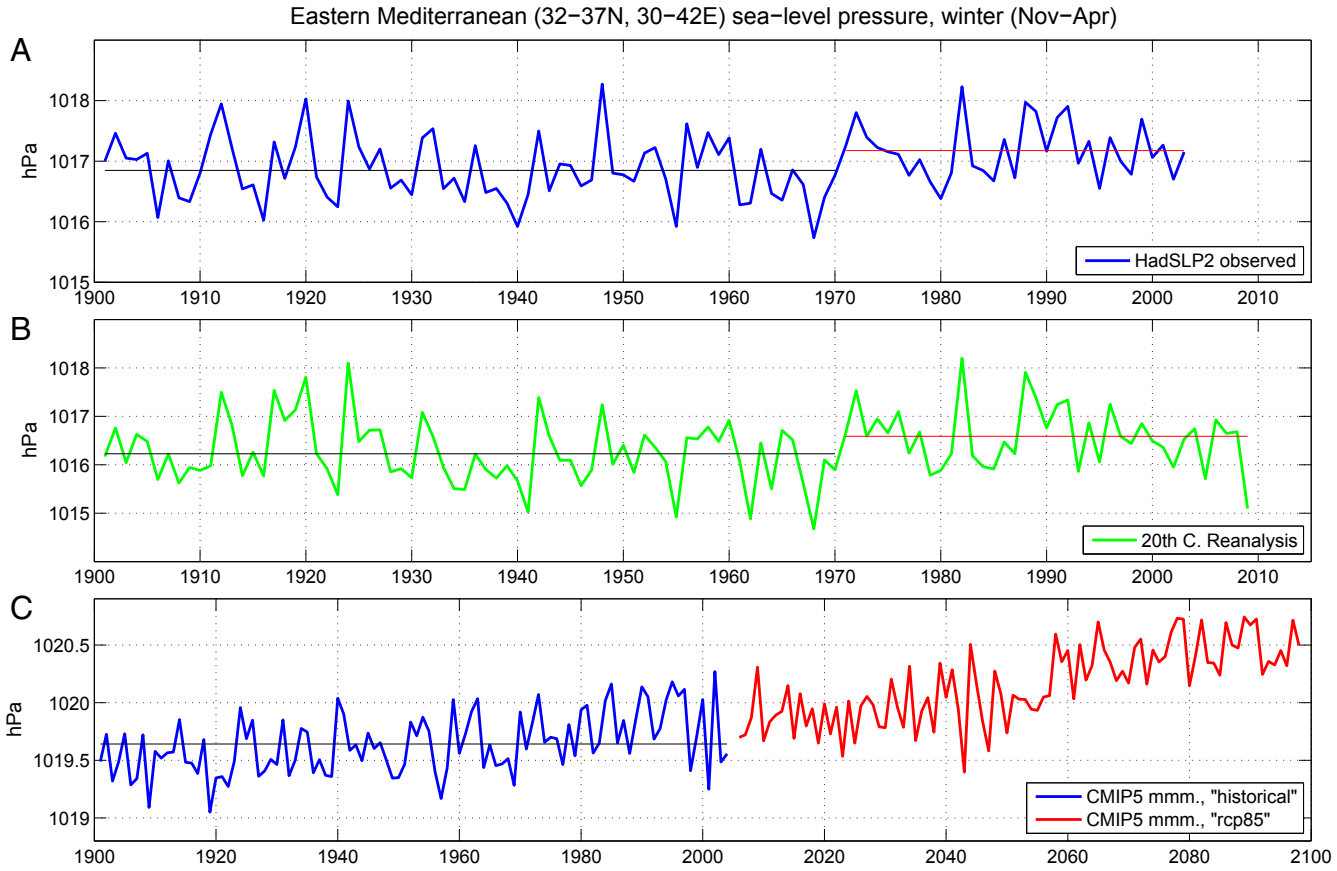

Fig. S4. Timeseries of area mean Eastern Mediterranean sea-level pressure for 6-month winter (November–April). (*A*) Observed HadSLP2, (*B*) 20th Century Reanalysis, and (*C*) CMIP5 multimodel mean (16 models; see Table S1) for the 20th century "historical" simulations and 21st century rcp85 projections.

Table S1. CMIP5 models used in this study

Model	Horizontal resolution, lon × lat	Modeling center
bcc-csm1-1	2.81 × 2.81	Beijing Climate Center, China Meteorolgical Association
BNU-ESM	2.81 × 2.81	College of Global Change and Earth System Science, Beijing Normal University
CNRM-CM5	1.41 × 1.41	Centre National de Recherches Meteorologiques
CSIRO-Mk3-6–0	1.88 × 1.88	Commonwealth Scientific and Industrial Research Organization
FGOALS-g2	2.81 × 2.81	State Key Laboratory of Numerical Modeling for Atmospheric Sciences and Geophysical Fluid Dynamics, Institute of Atmospheric Physics, Chinese Academy of Sciences and Center for Earth System Science, Tsinghua University
GFDL-CM3	2.5 × 2	National Oceanic and Atmospheric Administration (NOAA) Geophysical Fluid Dynamics Laboratory
GFDL-ESM2M	2 × 2.5	NOAA Geophysical Fluid Dynamics Laboratory
GISS-E2-H	2.5 × 2	NASA Goddard Institute for Space Studies
GISS-E2-R	2.5 × 2	NASA Goddard Institute for Space Studies
HadGEM2-ES	1.88 × 1.25	Met Office Hadley Centre
IPSL-CM5A-LR	3.75 × 1.89	Institut Pierre-Simon Laplace
IPSL-CM5A-MR	2.5 × 1.27	Institut Pierre-Simon Laplace
MIROC-ESM	2.81 × 2.81	Atmosphere and Ocean Research Institute (University of Tokyo), National Institute for Environmental Studies, and Japan Agency for Marine-Earth Science and Technology
MIROC-ESM-CHEM	2.81 × 2.81	Atmosphere and Ocean Research Institute (University of Tokyo), National Institute for Environmental Studies, and Japan Agency for Marine-Earth Science and Technology
MRI-CGCM3	1.13 × 1.13	Meteorological Research Institute, Japan
NorESM1-M	2.5 × 1.89	Norwegian Climate Centre

Models were linearly interpolated to a common 0.5 degree by 0.5 degree horizontal grid (the same grid as the CRU data) for intercomparison. lat, latitude; lon, longitude.